NUMERICAL SIMULATION OF THE LOADING CHARACTERISTICS OF STRAIGHT AND HELICAL-BLADED VERTICAL AXIS TIDAL TURBINES

Philip Marsh[1a], Dev Ranmuthugala[2], Irene Penesis[1] and Giles Thomas[3]

[1]National Centre for Maritime Engineering and Hydrodynamics, Australian Maritime College, University of Tasmania. Locked Bag 1395, Launceston Tasmania 7250, Australia
[2]National Centre for Ports and Shipping, Australian Maritime College, University of Tasmania. Locked Bag 1397, Launceston Tasmania 7250, Australia
[3]Dept. of Mechanical Engineering, University College London, Torrington Place, London WC1E 7JE
[a]Corresponding author: marshp@amc.edu.au. Locked Bag 1395, Launceston Tasmania 7250, Australia. Phone: (+61) 401 639 059

Abstract: The stress and deflection of straight and helical-bladed vertical axis turbines was investigated using hydrodynamic and structural analysis models. Using Double Multiple Streamtube (DMS) and Computational Fluid Dynamics (CFD) models, the hydrodynamic forces and pressures on the turbines were modeled for three rotational rates from startup to over speed conditions. The results from these hydrodynamic models were then used to determine stress and total deflection levels using beam theory and Finite Element Analysis (FEA) methods. Maximum stress and deflection levels were found when the blades were in the furthest upstream region, with the highest stresses found at the blade-strut joints for the turbines studied. The helical turbine exhibited on average 13% lower maximum stress levels than the straight-bladed turbine, due to the helical distribution of the blades around the rotational axis. All simulation models offered similar accuracy when predicting maximum blade stress and deflection levels; however for detailed analysis of the blade-strut joints the more computationally demanding CFD-FEA models were required. Straight-bladed, rather than helical turbines, are suggested to be more suited for tidal installations, as for the same turbine frontal area they produce higher power output with only 13% greater structural stress loading.

Keywords: Vertical Axis Turbine, Structural Loading, Stress and Deflection Computational Fluid Dynamics, Finite Element Analysis

1. Introduction

Existing studies of vertical axis turbines used for ocean power generation have concentrated primarily on hydrodynamics rather than structural analysis, as researchers have sought to maximise power output. To ensure longevity in marine environments however, detailed knowledge of turbine structural loading characteristics must be established. Although possible using strain gauges, Experimental Fluid Dynamics (EFD) studies to obtain loading are rarely performed. This fact, when combined with a general lack of turbine development over the last 15 years for both wind [1] and tidal turbines, has limited turbine usage. However, knowledge of turbine hydrodynamics and structural characteristics can be obtained by numerical simulation using methods such as coupled Computational Fluid Dynamics (CFD) and Finite Element Analysis (FEA) codes. Additional research into both hydrodynamics and structural characteristics using numerical techniques will further understanding of turbine operational characteristics.

Both straight and helical-bladed designs, as shown in Figure 1, are proposed by various researchers to generate power from the ocean's kinetic energy [2-5]. The designs differ in blade helicity, defined by the blade overlap angle Φ shown in Figure 1. Straight-bladed turbines have 0° blade overlap, whereas helical turbines use blades that are distributed around the rotational axis at a defined overlap angle of Φ. Previous research by the authors indicated that straight-bladed designs generated higher power output when compared to helical turbines of the same frontal area and blade section as a result of the inclination of the helical turbines blades to the inflow [2]. Conversely, helical turbine torque oscillation levels and mounting forces were reduced when compared to straight-bladed turbines, due to the distribution of the turbine blades around the rotational axis [2]. Comparisons of the influence of these factors on the structural loading characteristics of the two designs is currently unknown, as previous research into loading characteristics has concentrated primarily on straight-bladed turbine designs.

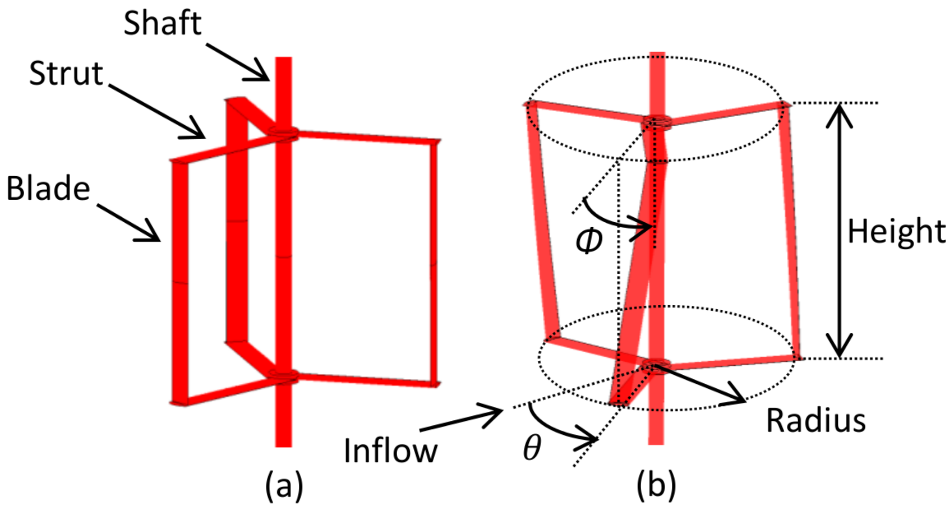

Figure 1: Straight (a) and helical-bladed (b) vertical axis turbines, showing definitions of azimuth rotational angle θ, and blade overlap angle Φ

Characterization of vertical axis turbine loading characteristics can be performed numerically by coupling Double Multiple Streamtube and CFD models with beam theory or FEA analysis methods [3-6]. However, considerable knowledge gaps exist in the characterisation of structural loading. Previous numerical studies have often been limited to either helical or straight-bladed designs [3-6], with no comparison between loading characteristics of the two designs performed. These works have often concentrated on blade loading, with no determination of the loading of the struts and blade-strut joints performed [3,5,6]. Additionally, previous simulations have concentrated on evaluating loading characteristics at a single rotational rate [3-6]. Research extending numerical simulation models to investigate straight and helical-bladed turbines using models with all geometrical features including struts at multiple rotation rates will give greater insight into turbine characteristics, and allow for the evaluation of any advantages between the differing geometrical layouts.

In this current study, the blade loading of a straight and a helical vertical axis turbine was determined to characterise blade and strut loading. The hydrodynamic inputs were generated using DMS and CFD models, which were combined with the application of centrifugal and gravitational forces to form structural analysis models using beam theory and FEA. Characterization of maximum stresses and deflection levels and their relationships with blade azimuth angle were performed. This work also sought to determine whether straight or helical turbines are more suited to generate ocean power from both hydrodynamics and structural perspectives.

2. Turbine Geometry

Two vertical axis turbine designs were simulated to evaluate the influence of variations of blade helicity on turbine structural loading characteristics. These models differed only in blade helicity as shown in Figure 1, with all common geometrical dimensions outlined in Table 1. Only two designs were considered: a straight-bladed turbine and a helical turbine with 15° of blade overlap. These were chosen as previous studies demonstrated that power output reduced significantly as blade overlap increased above 15° [2], reducing turbine utility for power generation. The geometrical layout of the straight-bladed turbine was based on an EFD turbine from literature to allow for validation of the numerical simulation techniques utilised [2,7]. The helical turbine used the same frontal area, strut geometry, blade chord, and blade section to allow comparisons between the two designs. Both turbines had two struts per blade located at the blade tips.

Table 1: Shared Geometry of the Straight and Helical Turbines

Geometry	Dimensions
Number of blades	3
Turbine height	0.685m
Blade section	NACA634021
Blade chord	0.065m
Blade overlap	0°
Radius	0.457m
Strut section	NACA0012
Strut chord	0.065m
Number of struts per blade	2
Shaft diameter	0.048m

3. Numerical Simulation Methods

Three loading simulation models were developed allowing for comparisons of the respective benefits of each numerical simulation technique. The simulation models were performed in two steps, first the hydrodynamics followed by the structural simulations. The models developed were the:

- DMS-Beam, DMS blade forces combined with a beam theory model;
- CFD–Beam, CFD blade forces combined with a beam theory model; and
- CFD-FEA, CFD model coupled to the FEA model using pressure mapping techniques.

3.1 Hydrodynamic Simulations

Numerical simulations of the hydrodynamic forces were performed using DMS and CFD simulation models. For both models, force coefficients normal to the blade chord were determined, with the forces non-dimensionalised by dynamic pressure and blade chord. The CFD model was also used to output surface pressure data for use with the coupled CFD-FEA model.

3.1.1 Double Multiple Streamtube (DMS) Model

The normal blade force coefficients were modeled using a DMS model previously developed by the authors based on the methods outlined in literature [9]. The turbine was modeled using a double actuator disk method to account for reductions in flow velocity through the streamtube from V_1 to V_2 as shown in Figure 2, with no streamtube expansion modeled for simplicity. Using iterative methods upstream and downstream, induction factors were calculated from which blade angles of attack were determined. Once the latter were known, the forces normal to the blade chord were determined using lift and drag data obtained using the viscous airfoil analysis tool Xfoil [9]. As NACA634021 data was not readily available from literature at suitable Reynolds numbers, NACA634221 data was used as it was similar in profile, with a 2% difference in blade camber. The DMS model included dynamic stall modeling using the Gormont method to simulate the influence of the variations in blade angles of attack generated by the rotation of the blades [10]. Currently the DMS model developed by the authors cannot model helical turbines, as the hydrodynamic influence of the blade inclination has not been adequately accounted for.

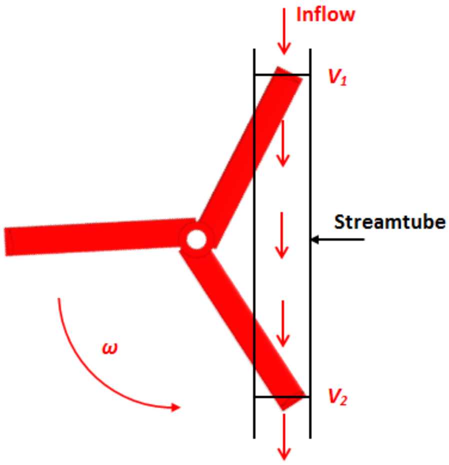

Figure 2: DMS model showing an example of the streamtube method for calculation of upstream and downstream flow velocity values V_1 and V_2

3.1.2 Computational Fluid Dynamics (CFD) Models

Turbine blade forces were simulated using transient time-accurate 3D CFD models using ANSYS CFX [11], which solved the incompressible fully turbulent URANS equations using an element-based finite volume method. All turbine models were meshed using unstructured tetrahedral elements using ANSYS CFX 13.0 [12-15]. Mesh resolution was set by specifying the mesh size and growth rates to allow for local refinement of mesh zones, with inflation layers used on all surfaces to fully resolve the surface boundary layer flow [12-15]. Turbine rotation was simulated by enclosing the turbine in an inner domain as shown in Figure 3 that was rotated using the CFX transient rotor-stator model at the desired rotational rate. The interface between the stationary and rotating domains was modeled using a General Grid Interface (GGI) over which flow values are calculated using an intersection algorithm [11].

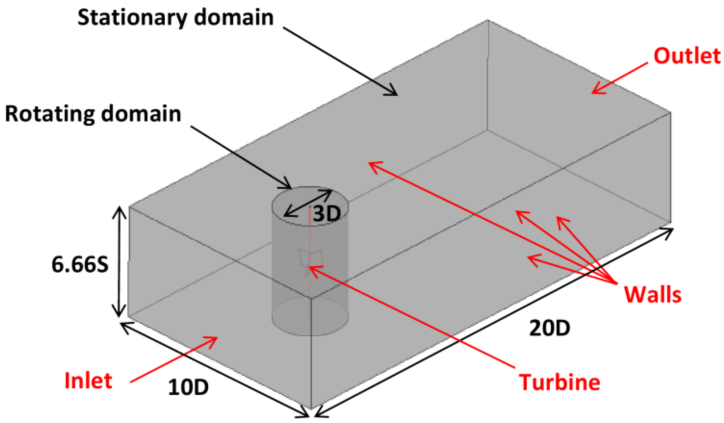

Figure 3: Simulation domain boundary nomenclature and sizing used for straight and helical CFD models. Dimensions in relation to turbine diameter, D, and height, S, as shared by the two turbine designs

The computational domains shown in Figure 3 were generated to simulate free stream conditions, with all corresponding boundary conditions outlined in Table 2. To ensure that the turbines were isolated from any domain wall effects and to allow for full wake development, systematic domain size studies were performed [2,12-15]. All turbines were assumed to operate at sufficient depth to minimise any free surface interaction effects, and thus only the water phase was modeled.

Table 2: Boundary Conditions for the Straight and Helical Turbines

Boundary	Condition
Inlet	Uniform flow: 1.5 ms^{-1}
Inlet turbulence level	5% turbulence
Outlet	Relative pressure: 0 Pa
Walls	Free slip walls
Turbine	No slip walls

The *k-ω* SST turbulence model was utilised for turbulence closure due to its ability to accurately model both free stream and boundary layer regions as well as offering improved prediction of flow separation and adverse pressure gradients by the inclusion of transport effects into the formulation of the eddy-viscosity [16], with the *k-ω* SST CFD turbulence model commonly used for vertical axis turbine simulations [2,12-15,17-21]. To ensure numerical accuracy and stability, all simulations were performed using a high order advection and second order transient scheme [12-15]. Convergence was deemed achieved when solution residuals reduced to below 10^{-4} and reduced by more than three orders of magnitude.

Studies of the influence of factors including mesh density, time step size, *y+*, domain length, width and height were conducted. Independence was deemed satisfactory when significant increases in these parameters resulted in C_p differences between successive refinements trending to less than 5%. This resulted in a suitable balance between solution accuracy and computational effort. Full mesh convergence studies were conducted by the authors for the straight and helical-bladed turbine simulated in this work and were presented previously in [2,12-15].

3.1.3 Hydrodynamic Model Validation

Validation of CFD methods against EFD testing of a one and three-bladed turbine from literature revealed good agreement for normal force coefficient predictions [22,23]. The CFD maximum normal force coefficients were predicted on average to within 5.7% of EFD [22,23], with the relationship with rotational angle replicated accurately. The DMS model was able to accurately predict the location of the maximum normal force as shown in Figure 4, however it under-predicted the normal force on average by 40% as a result of severe dynamic stall effects that the Gormont dynamic stall model was unable to satisfactorily capture.

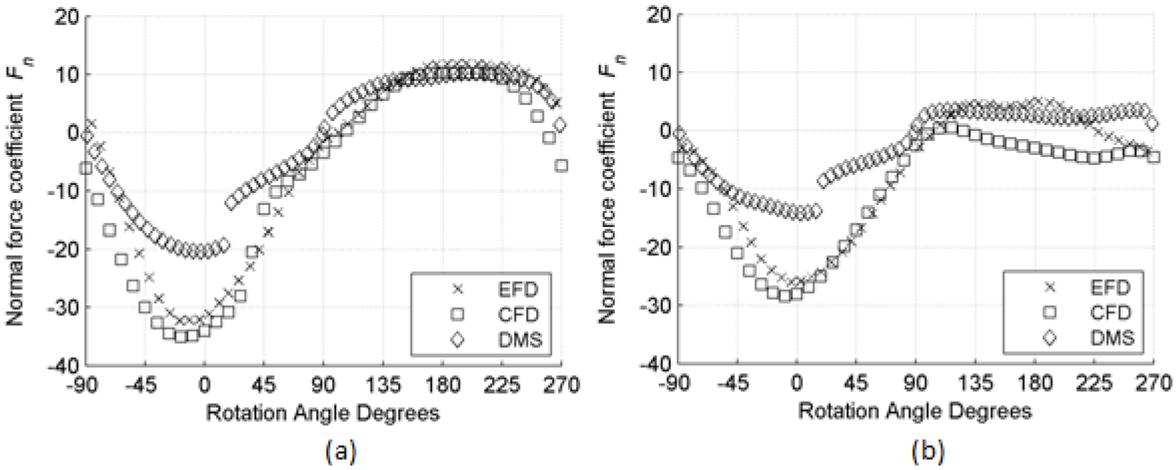

Figure 4: Normal force coefficients for the (a) one-bladed and (b) three-bladed turbines compared to EFD results [22,23] at a rotational rate of 0.746 rads^{-1} and an inflow velocity of 0.091 ms^{-1}

3.2 Structural Simulations

Two numerical simulation models were utilised to characterise turbine loading characteristics; beam theory and FEA models. These models used either force or pressure field results from the DMS and CFD models outlined in Section 3.1. The beam theory model simulated the structural loading using a simply supported model, whereas the FEA model simulated the entire turbine structure including the rigid blade-strut joints. The influence and limitations of these differing structural simulation approaches was investigated as part of this work.

3.2.1 Beam Theory Model

A beam theory model was developed using code scripted in Matlab. Three key assumptions were made to allow the use of this approach. The normal force was assumed to be uniformly distributed to simplify the coupling between the hydrodynamic and structural models, although the actual force distribution may be reduce near the tips of the blades due to blade end and blade-strut interaction effects. The normal force was also assumed to contribute the most to blade stress and deflection, as normal forces are on average an order of magnitude greater than the tangential forces [8]. The normal force also acts in the direction normal to the blade chord line, resulting in large bending moments when compared to the small bending moments caused by the tangential forces. The blades were also assumed to be simply supported at each end, resulting in the assumption that the stress at the blade ends was zero as beam models were unable to model the stress at the blade-strut joints due to the geometrical layout of vertical axis turbines. The beam theory models were developed to establish their accuracy when compared to CFD-FEA models in the simulation of blade stress and deflection as they require considerably less computational requirements and solutions times.

To calculate the blade stress and deflection, first the normal force coefficients are determined using the DMS or the CFD models. The forces determined are then transformed into a uniformly distributed load across the span of the blade. The centrifugal force F_c caused by the turbine rotation is found as,

$$F_c = m\omega^2 r \tag{1}$$

where *m* is the blade mass, *ω* is the rotational rate, and *r* is the turbine radius. The distributed load, *w*, acting on the blade span is the sum of hydrodynamic and centrifugal forces calculated. Using this total load, the bending moment, *M* is calculated using simple beam theory, where the bending moment is obtained as,

$$M = \frac{w{l_e}^2}{8} \tag{2}$$

where l_e is the blade span. The maximum stress, *σ*, is determined using,

$$\sigma = \frac{My}{I} \tag{3}$$

where *y* is half the maximum blade thickness, and *I* is the area moment of inertia determined using a simple approximation for hydrofoil sections [24] given by,

$$I = K_1 c^4 t(t^2 + \varepsilon^2) \tag{4}$$

where K_1 is a derived proportional coefficient, *c* is the blade chord, *t* is the blade thickness, and *ε* is the camber percentage. The blade deflection is calculated using,

$$Deflection = \frac{5w{l_e}^4}{384EI} \tag{5}$$

where *E* is the material modulus of elasticity.

3.2.2 Structural Finite Element Analysis (FEA) Model

The stress and deflection on turbine blades and struts were evaluated using the ANSYS FEA linear Static Structural analysis module [25]. The hydrodynamic pressures on the blades were calculated by the CFD models and mapped on to the structural model surfaces using Octree mapping [25], as shown in Figure 5. Additionally, inertia and gravitational loads were included to model the steady inertial loads. The FEA model was constrained at the shaft and hubs to allow for evaluation of the blade and strut forces, reducing computational effort. Unlike the DMS-Beam model, the CFD-FEA model allowed for the determination of stress and deflection levels in both the blades and struts. The von Mises stress and total blade deflections were calculated at each turbine azimuth angle using a custom Python script written by the authors. This script loaded the surface pressure fields from the CFD transient analysis for each time step, enabling a one-way Fluid Structure Interaction (FSI) simulation, as any deflections calculated were not reverted back to the CFD model. Two-way FSI techniques were examined, however due to their excessive simulation time they were not considered feasible, unless mesh element count was reduced which would adversely affect the accuracy of the hydrodynamic simulations. The simulated turbines were constructed from steel with all material properties shown in Table 3.

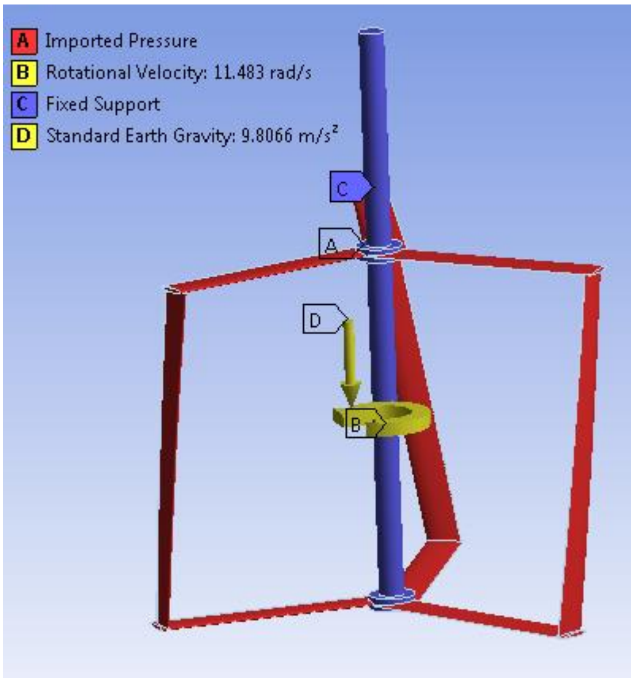

Figure 5: ANSYS structural model of helical turbine showing loading conditions including imported pressures, rotational velocity, gravity, and the fixed supports

Table 3: Material properties used for straight-bladed and helical turbine structural analysis

Material	Steel
Density (kg/m^{3})	7850
Tensile Yield Strength (MPa)	250
Compressive Yield Strength (MPa)	250
Ultimate Tensile Strength (MPa)	460
Young's Modulus *E* (GPa)	200

The geometry of the FEA turbines was identical to that used in the CFD models, except for the addition of fillets at the blade-strut joints. Fillets of 0.0025m radius were added to avoid infinite or singular stress concentrations at the re-entrant corners of the joints. These can occur as forces applied to mesh cells of reducing size at the fillets will result in ever-increasing stress predictions as the mesh area reduces. To ensure that the addition of fillets did not influence simulation accuracy, maximum von Mises stress magnitudes were determined using CFD models with and without fillets. Variations of maximum stress of less than 1.5% were determined, allowing the use of de-featured CFD models to increase computational efficiency.

Mesh convergence studies were performed to verify all FEA meshing techniques utilised, with independence studies for maximum and minimum mesh sizing, face sizing refinement, growth rate, and curvature angle performed. Mesh convergence found to be highly dependent on the face sizing of the fillets between the blades and strut joints where the maximum stress magnitudes were located. Successive mesh refinement demonstrated mesh element count independence at 143,000 elements.

4.0 Results and Discussion

The loading characteristics of straight and helical-bladed turbines were investigated using the DMS-Beam, CFD-Beam, and CFD-FEA models. For each model, stress levels and total blade deflections were recorded over one rotation. All results were simulated at an inflow velocity of 1.5 ms^{-1}. Simulations of turbine loading characteristics were performed for three rotational rates representative of common turbine operational ranges corresponding to a rotational rate of:

- λ=1.5 similar to that found when starting the turbine;
- λ=2.75 corresponding to the maximum power output; and
- λ=3.5 representing an over speed condition.

where λ is the tip speed ratio defined as,

$$\lambda = \frac{rw}{V} \tag{6}$$

and V is the inflow velocity.

4.1 Normal and Tangential Force Coefficients

Using the DMS and CFD models, the normal force coefficients for the straight three-bladed turbine shown in Figure 1 were obtained at λ=1.5, 2.75, and 3.5 as shown in Figure 6. For λ=1.5 agreement between the two numerical methods was very good, with both the relationships with azimuth angle and the normal force coefficient magnitudes for each model agreeing closely. The maximum force coefficients were found to occur at approximately -22.5° by both numerical models, with the definition of rotational angle shown in Figure 1. This was due to peaks in the lift generated by the favorable angle of attack over the blades and dynamic stall effects at this azimuth angle. Differences in maximum force of 8.5% were determined between the two models, which may be attributed to differences in dynamic stall modeling, as these differences were found around the force coefficient peaks. The normal force coefficients in the downstream region from 90° to 270° were not fully reversed when compared to the upstream region, as a result of reductions in the flow velocity over the downstream blades caused by the preceding blade's wake. Large reductions in force in the downstream region were previously found in EFD and CFD studies, with force magnitudes of less than 1/3 found when comparing peak values with average values in the downstream region [22,23].

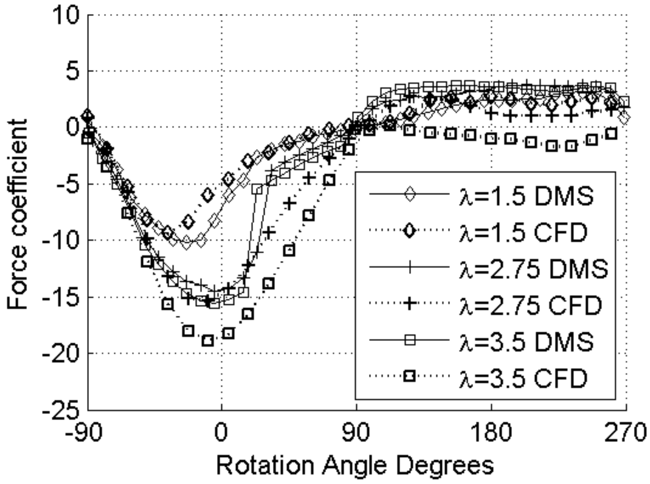

Figure 6: Normal force coefficient simulations for one revolution using the DMS and CFD models at λ=1.5, 2.75, and 3.5

Figure 6 also compares simulations of normal force coefficients using the DMS and CFD models at λ=2.75. Maximum force coefficient predictions for both models at λ=2.75 were within 7.3%, with the location of the maximum force predicted at the same azimuth angle for both models. Although the shape of the simulated normal force coefficient curves was similar, predictions of normal force coefficient diverged in the downstream region around 180°. The DMS model accounted for reductions in flow velocity in the downstream region, but it did not account for the increased levels of turbulent flow over the downstream blades, which reduces lift and hence normal force coefficients. However, these turbulent flow effects were simulated by the CFD model, resulting in discrepancies between the two models in the wake-influenced downstream regions. The jump in force coefficient around 22.5° to 45° was caused by jumps in the lift and drag tables used in the DMS model, as well as the by the rapid reduction in the additional lift determined by the dynamic stall model.

Figure 6 also shows the normal force simulations at λ=3.5 as determined using the DMS-Beam and CFD-Beam models. The predicted azimuth location of maximum force coefficients agreed well, however reduced correspondence was found when comparing maximum force coefficient values predictions, which were within 21% of each other. This reduction in force coefficient similarities between the numerical models when compared to the λ=1.5 and 2.75 results may be due to the over prediction of the increasing influence of strut drag on the turbine as λ increases by the DMS model. Similar to the simulations of normal force coefficient at λ=1.5 and 2.75, differences in the downstream region between the CFD and DMS model were apparent.

4.2 Straight-Bladed Turbine Loading and Deflection Simulations

Figure 7 compares von Mises blade stress and deflection levels at λ=1.5 for the DMS-Beam, CFD-Beam, and CFD-FEA models. The CFD-FEA blade results ignored the stress concentrations at the blade-strut joints, allowing comparison between the simulation models. The highest blade stress and deflection levels were found around -22.5° coinciding with the peaks in the normal force coefficients shown in Figure 6. Similarities across all λ were found between the three simulation models, with the location of maximum stress and deflection found mostly at the middle of the blade span. The maximum stress and total deflection results determined using the DMS-Beam and CFD-Beam models were within 8.4% of each other, as they were calculated using similar values of normal force coefficient as shown in Figure 6. At high absolute values of force coefficients the DMS–Beam and CFD–Beam results diverged from the CFD-FEA simulations due to differences in the structural support conditions at the blade ends. In the CFD model the deflection of the struts reduced the blade stress levels, whereas the beam theory models assumed that the blade was simply supported, resulting in increased stress levels. The stress on the blades was cyclic; however it is not fully reversed, with reduced levels found in the downstream region around 180°.

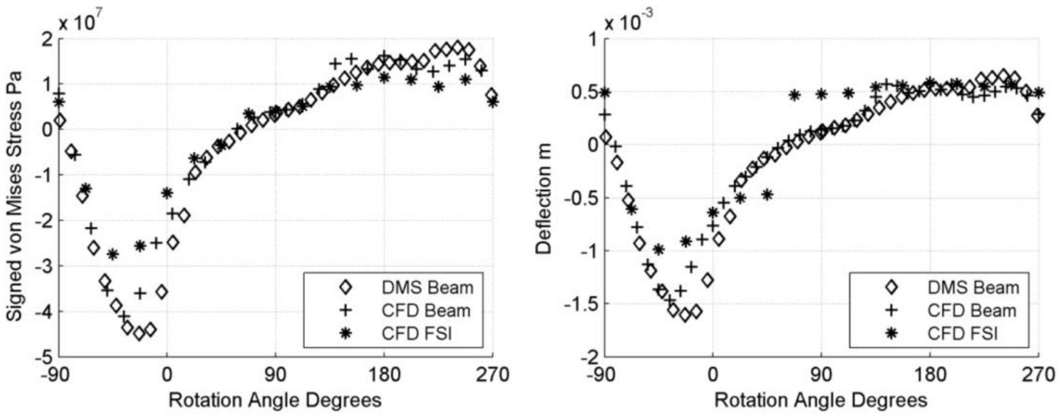

Figure 7: Signed maximum von Mises blade stress and total deflection comparisons for the DMS-Beam, CFD-Beam, and CFD-FEA straight-bladed turbine models at λ=1.5. Positive deflection is outwards away from the shaft

Comparisons of blade von Mises blade stress and deflection at λ=2.75 are shown in Figure 8. The three simulation model curves prescribe similar stress and deflection curves, with maximum values located at the middle of the blade span. The highest stress and blade deflection was found at approximately 0°, with peak stress loads increased on average by 45% when compared to the λ=1.5 case. This increase in stress was caused by increases in blade lift due to the blade angle of attack variations reducing to more favorable levels below stall as λ increased. Similar to that found at λ=1.5, the DMS-Beam and CFD-Beam models differed in maximum stress level prediction from the CFD-FEA model, as a result of the blade end support conditions. The von Mises stresses were not fully reversed, due to reductions in flow velocity and increased flow turbulence generated by the wake of the upstream blades. The DMS model predicted higher stress and deflection levels in the downstream regions, as it was unable to simulate the influence of this upstream blade vortex shedding on the downstream blades.

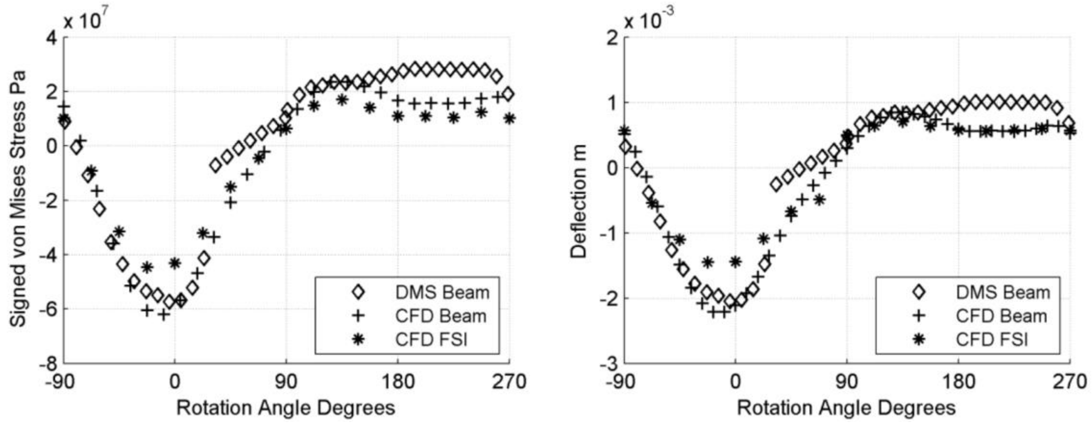

Figure 8: Signed von Mises blade stress and total deflection comparisons for the DMS-Beam, CFD-Beam, and CFD-FEA straight-bladed turbine models at λ=2.75. Positive deflection is outwards away from the shaft

Figure 9 shows the simulated von Mises blade stress and total deflection at λ=3.5, with the maximum values located at the middle of the blade span. The maximum stresses were found at approximately 0°, as a result of peaks in normal force coefficient in the upstream region as shown in Figure 6. Peak stress values were found to increase on average by 10.6% when compared to the λ=2.75 case. This increase was less than that found between λ=1.5 and 2.75, as the increase in λ resulted in increased centrifugal forces on the blades which oppose the hydrodynamic forces in the upstream direction. Similar to results in Figures 6 and 8, the maximum stress levels simulated by the CFD-FEA model were reduced when compared to the DMS and CFD-Beam Theory models.

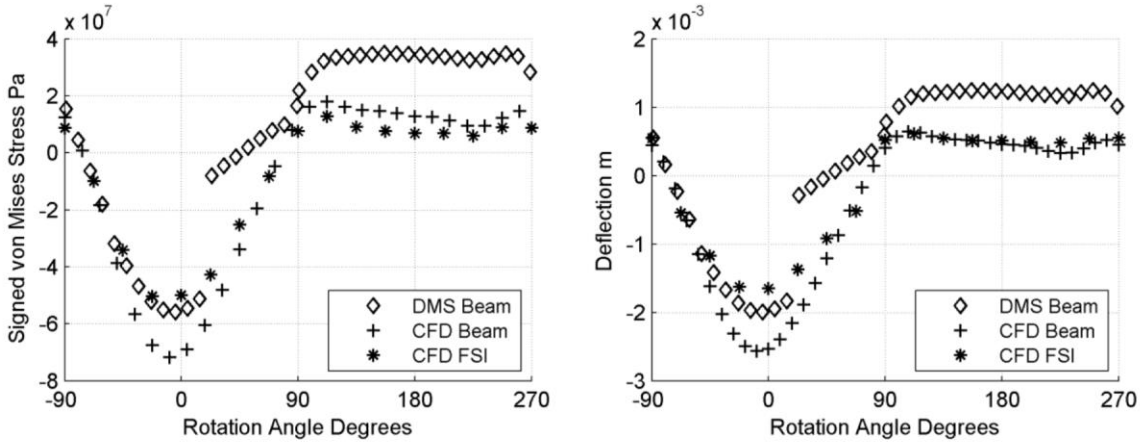

Figure 9: Signed von Mises blade stress and deflection comparisons for the DMS-Beam, CFD-Beam, and CFD-FEA straight-bladed turbine models at λ=3.5. Positive deflection is outwards away from the shaft

For all simulation models, the highest magnitude of the blade deflection versus blade span was 0.4%. The small blade deflections found would have minimal impact on the lift and drag generated over the blade, allowing one-way FSI models to be used. However, if the turbine was constructed from a more flexible material with a lower modulus of elasticity, these deflection levels would be much higher as a percentage of the blade span, possibly requiring a two-way FSI approach.

Figure 10 illustrates strut and blade deflection over one rotation using the CFD–FEA model. The blades can be seen to deflect inwards between the rotational angles of -90° to 45°, after which they deflected outwards for the rest of the rotational cycle. This cyclic pattern repeats over each revolution, generating tension and compression cycles on the blades. The struts can also be seen to deflect with the blades, particular at the blade-strut joints.

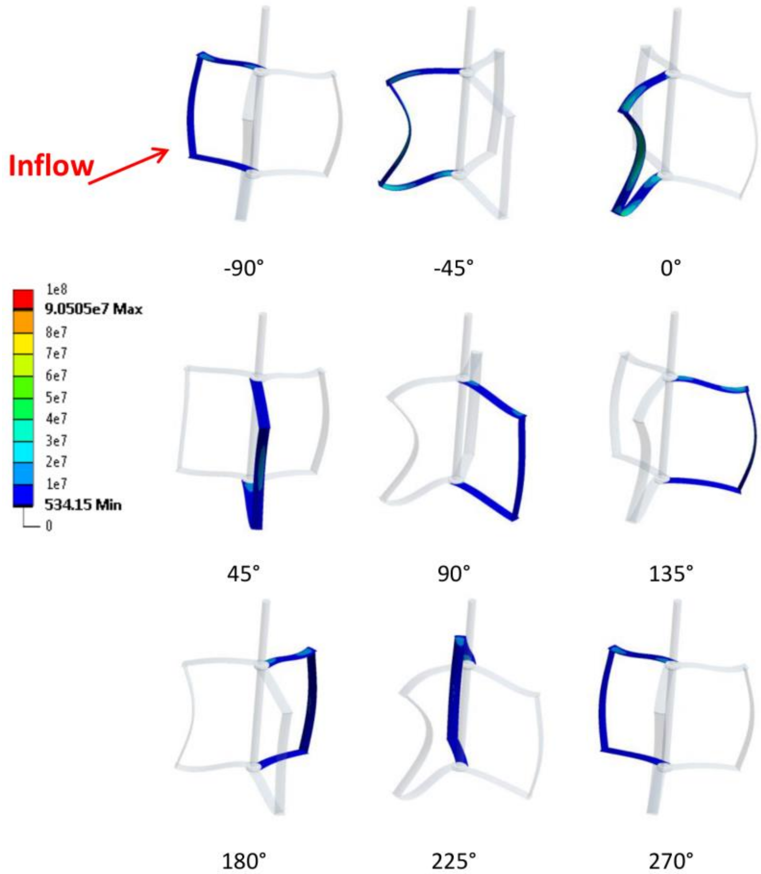

Figure 10: Turbine von Mises stress magnitudes for one turbine rotation at λ=2.75. Deflection scale increased by 150 to highlight structural deformation

The centrifugal forces generated by the turbines rotation opposed the hydrodynamic forces in the upstream region from approximately -90° to 90°, reducing blade stress and deflection levels, whereas in the downstream region from 90° to 270° the hydrodynamic and centrifugal forces combined. However, the hydrodynamic normal blade forces in the downstream region were significantly reduced when compared to upstream normal force values as shown in Figure 6, due to the reduction in flow velocity in the downstream region and the turbulent flow effects of the preceding blades wake. Thus, the combined downstream total hydrodynamic and centrifugal forces and hence blade stress and deflections were reduced when compared to upstream values. For the turbines studied here the hydrodynamic force was dominant, with upstream force magnitudes and hence blade stress and deflection levels higher than downstream values for all λ simulated.

The CFD-FEA model was then used to predict the maximum stress magnitudes within the blades and the struts. The maximum stress was found to occur at the bottom blade-strut joint for all λ, as a result of the combination of hydrodynamic and gravitational loading, with levels significantly higher than blade stress levels shown in Figures 7, 8 and 9. An example at λ=2.75 is shown in Figure 11, with results in Figure 12 showing the maximum stress relationships with azimuth angle for each λ simulated. The maximum stress occurred at approximately 0° at the bottom blade-strut joint, as the maximum normal force occurs at this azimuth angle as shown in Figure 6. These normal force peaks generated large bending moments, and hence large stress concentration at the blade-strut joints, with peak magnitudes of approximately 101 MPa noted. The use of beam theory models will not resolve this depending on the location of the strut on the blades.

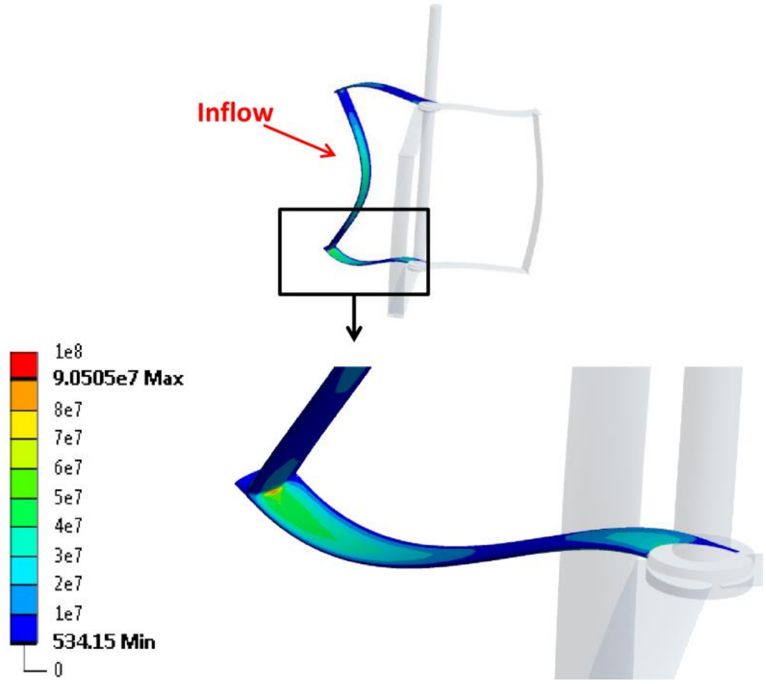

Figure 11: Stress concentration at bottom blade-strut fillet showing the location of maximum von Mises Stress of 90.51 MPa at the azimuth angle of 0° at λ=2.75

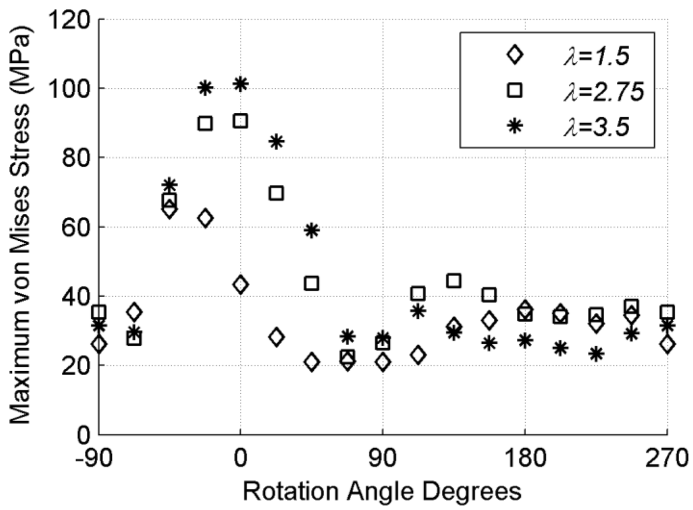

Figure 12: Maximum von Mises Stress at the bottom blade-strut fillet over one revolution determined using the straight-bladed CFD-FEA turbine model at λ=1.5, 2.75, and 3.5

Comparison of yield safety factors are shown in Figure 13, where the yield safety factor was defined as the ratio of the material yield stress shown in Table 3 to the maximum stress. For each λ, the maximum stress levels were below the material yield strength, with minimum safety factors of 3.84, 2.76, and 2.49 found for λ=1.5, 2.75, and 3.5. However, the analysis of yield safety factors does not take into consideration any fatigue issues as a result of the cyclical loading. If the tidal velocity distribution is known, the models developed here can be used to determine the fatigue life of turbine using rainflow counting methods combined with fatigue models such as Miners rule [26].

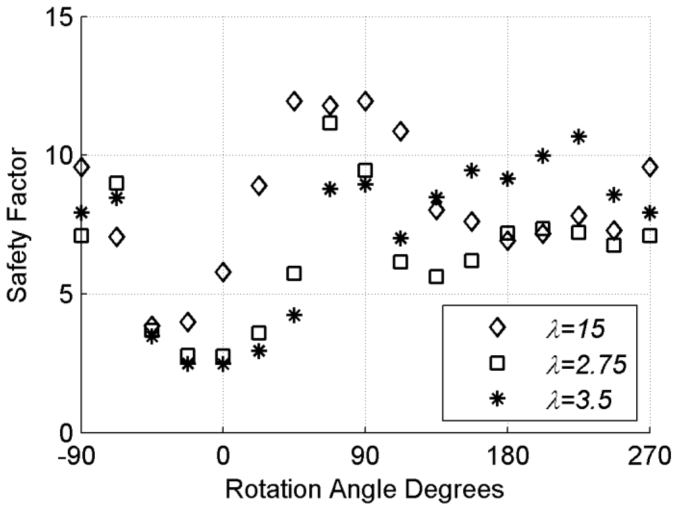

Figure 13: Yield safety factor for the straight-bladed CFD-FEA simulation results for one revolution at λ=1.5, 2.75, and 3.5

4.3 Helical Turbine Normal Force Coefficients

Using the CFD model, the normal blade coefficients were determined for the helical turbine at λ=1.5, 2.75, and 3.5 as shown in Figure 14. Similar to the coefficient curves determined for the straight-bladed turbine shown in Figure 6, maximum force was found at approximately -45° to -22.5°. The normal force coefficients for the helical turbine shown in Figure 14 were reduced when compared to the values found for the straight-bladed turbine shown in Figure 6, as the distribution of the helical blade around the rotational axis does not generate lift force peaks simultaneously along its full length as it rotates in the upstream section at azimuth angles from -90 to 0°.

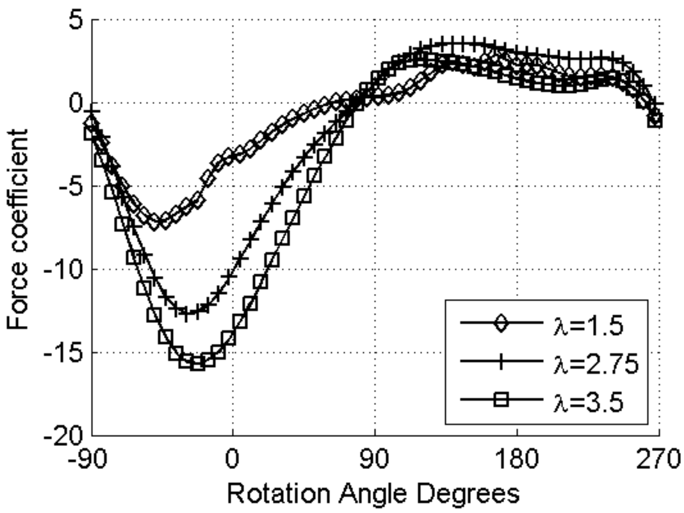

Figure 14: Normal force coefficient simulations for one revolution for the helical CFD model at λ=1.5, 2.75, and 3.5

4.4 Helical Turbine Loading and Deflection

Figure 15 shows the helical turbine von Mises blade stress magnitudes and deflection using the CFD-FEA analysis model. These results focused on the blades and ignored the stress concentrations at the blade-strut joints to allow for comparison with the blade force simulations shown in Figures 7, 9, and 10. Peaks in stress and total deflection occurred for all λ at approximately -45° to -22.5°, with the blades deflected inwards by up to 0.0014 m. In the downstream region the blade deflected outwards, however the stress magnitudes were not fully reversed, similar to that found for the straight-bladed turbine. The helical blade stress and deflection levels were reduced when compared to the straight-bladed turbine results shown in Figures 7, 8 and 9 as the normal force coefficient levels were lower, shown when comparing CFD force predictions in Figures 6 and 15.

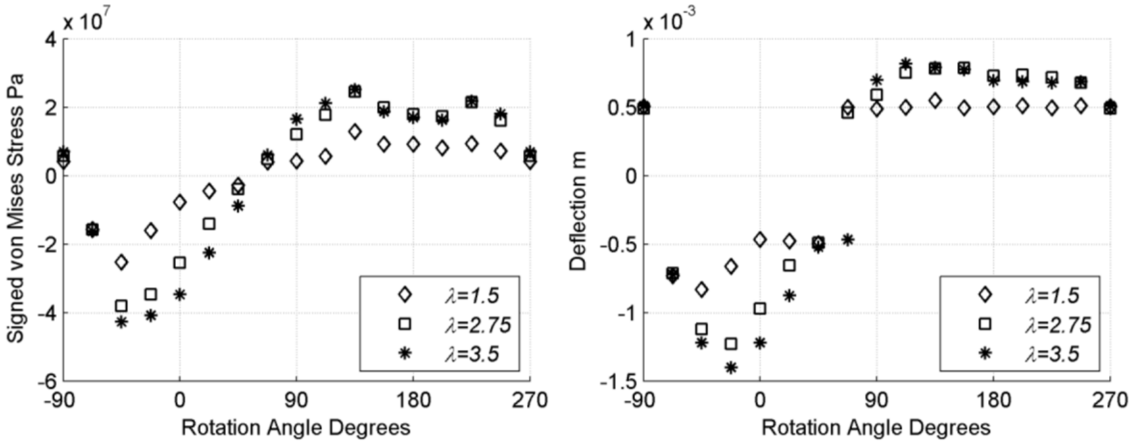

Figure 15: Helical turbine signed von Mises blade stress and deflection comparisons found using CFD-FEA models at λ=1.5, 2.75, and 3.5. Positive deflection is outwards away from the shaft

Figure 16 compares the blade and strut maximum von Mises stress magnitudes at λ=1.5, 2.75, and 3.5. Similar to the straight-bladed turbine results shown in Figure 11, stress peaks occurred at the bottom blade–strut joint due to the combination of hydrodynamic and gravitational forces. Peaks in maximum stress levels were found to occur at azimuth angle of -45° to -22.5°, due to the peaks in normal force generated by the blade in the upstream regions.

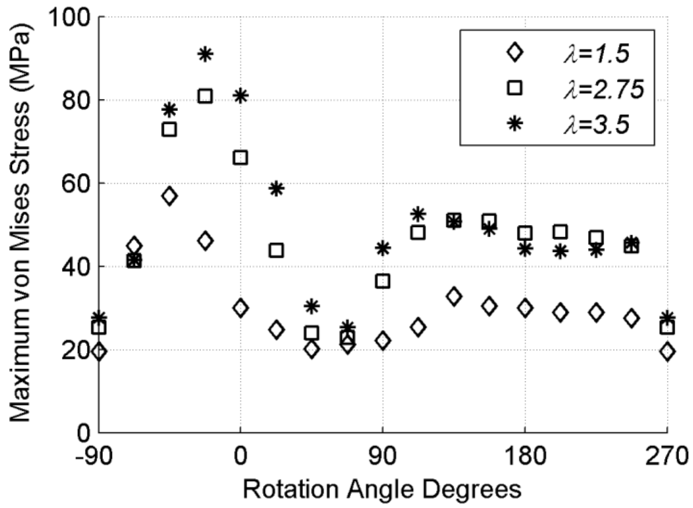

Figure 16: Maximum helical-bladed turbine von Mises stress levels comparing λ=1.5, 2.75, and 3.5

4.5 Straight and Helical Bladed Turbine Loading Comparisons

Comparisons of maximum von Mises stress levels for the straight and helical turbines are shown in Figure 17. For all λ, the straight-bladed turbine maximum stress levels were approximately 12.9% higher than for the helical turbine values. The straight-bladed turbine stress peaks were higher as the blade generates peaks in lift along its full length simultaneously, whereas the helical turbine blade lift peaks occur along the blade span at differing rotational angles due to the blades distribution around the rotational axis. The decrease in blade bending moment levels found for the helical turbine reduces blade stress when compared to the straight-bladed turbine. In addition, the moment of inertia of the helical blades is better suited to resist bending when compared to the straight blades, again due to their distribution around the rotational axis. Similarly, the blade stress and deflection levels of the helical-bladed turbines were lower than that of the straight-bladed turbines for all λ.

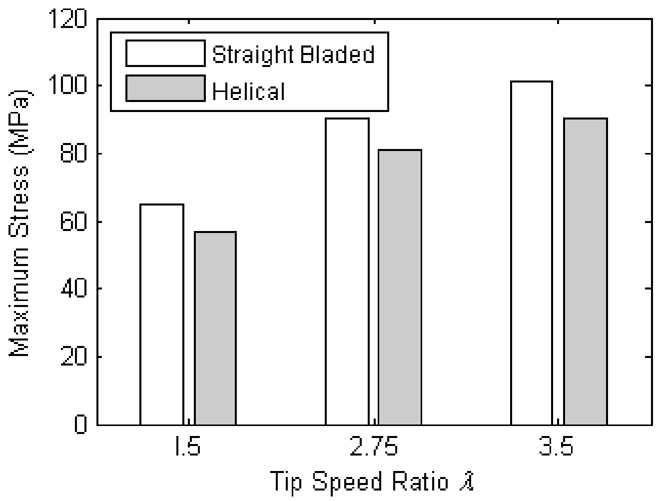

Figure 17: Comparisons of the maximum von Mises Stress magnitudes determined using the CFD–FEA models for the straight and helical turbine models at λ=1.5, 2.75, and 3.5

For ocean and tidal power installations, the authors suggest that straight-bladed turbines are more suitable than helical-bladed turbines as they generate 8% more power for the same frontal area [2], without any significant increase in stress levels as shown in Figure 18. These factors will increase installed power generation capacity while not reducing turbine longevity. Additionally, straight-bladed turbines are much simpler to manufacture than the curved blades of helical turbines, reducing blade manufacturing costs.

Although no EFD data was available to validate force coefficient simulations for the DMS and CFD models, close agreement between the two models provides some verification and gives confidence in the predicted results. Although the two numerical methods use different techniques, one based on EFD lift and drag data tables and the other on solutions to the Navier-Stokes equations, the normal force coefficient predictions found were on average within 12% of each other for all rotational rates. Combined with the previous validation of the DMS [13] and CFD [2,12-15] models, this high level of agreement gives confidence in the hydrodynamic simulation results presented in this paper. Additionally, although no validation data was available for the structural simulations, the level of agreement between the predicted blade stress and deflection results through the use of two separate structural analysis methods gives confidence in the results presented.

4.6 Computational Requirements

Significant differences in total simulation time and files sizes were required between simulation models as shown in Table 4. All numerical solutions were performed on an Intel i7 860 2.8 GHz based cluster with 2GB ram per core. The significant variations in simulation time suggest that the turbine design process should be performed in two stages. For initial geometrical design studies DMS-Beam models allow the quick estimation of normal forces, blade stress, and deflection levels; enabling the optimization of both power output and blade loading. However, the determination of maximum stress magnitudes as found at the blade-strut joints required the use of CFD-FEA models, as beam theory-based models were unable to resolve the blade-strut stresses.

Table 4: Computational Requirements for One Revolution of the Straight-Bladed Turbine at λ=2.75

Model	Hydrodynamic	Cores	Structural	Cores	File Size
DMS-Beam	1 minute	1	1 minute	1	1 Mb
CFD-Beam	2400 minutes	24	1 minute	1	80 Gb
CFD-FEA	2440 minutes	24	500 minutes	2	160 Gb

Simulations using coupled two-way FSI models were attempted, however they were not completed as it was estimated that the simulations would take around 140 days to complete one revolution, due to the combination of large CFD mesh element counts and reductions in numerical speed due to the coupling of the CFD and FEA models. This compared poorly with the one-way FSI simulations reported here, with total run times of less than 2 days.

5. Conclusions

Numerical evaluations of the hydrodynamic and structural loading of straight and helical-bladed turbines were performed using DMS, CFD, beam theory, and FEA methods. These simulations were performed at multiple rotational rates to characterise blade and strut loading. This study revealed three key findings:

- straight-bladed turbines exhibit higher maximum stress and deflection levels than helical turbines;
- maximum stress levels were found at the bottom blade-strut joints for both straight and helical-bladed turbines; and
- maximum stress levels for straight and helical turbines were well below yield strength at an inflow velocity of 1.5 ms^{-1}.

Combined, the key outcomes listed above lead to an important finding; that straight-bladed turbines are better suited for ocean power than helical turbines, as they generate higher power output without any significant increases in blade loading.

The simulation models developed in this paper open up considerable possibilities to improve vertical axis turbine designs from both hydrodynamic and structural perspectives. Based on this work the following is recommended:

- investigate blade-strut joint designs using FEA to reduce maximum stress concentration levels; and
- conduct EFD using strain gauges to evaluate turbine loading characteristics and provide validation data for the models developed in this work.

Nomenclature

c	Blade chord (m)	V_1	Upstream Velocity (ms^{-1})
E	Youngs modulus (Pa)	V_2	Downsteam Velocity (ms^{-1})
F_c	Centrifugal force (N)	w	Distributed load (kg/m)
K_1	Moment of interia proportonality coefficient	y	Maximum blade thickness /2 (m)
l_e	Effective Blade Length (m)	ε	Blade camber (%)
I	Area moment of interia (m^4)	λ	Tip speed ratio
m	blade mass (km)	σ	Blade stress (Pa)
M	Blade moment (Nm)	ρ	Density (kgm^{-3})
r	Radius (m)	τ	Blade thickness (%)
S	Turbine Frontal Area (m^3)	Φ	Blade overlap angle (degrees)
V	Inflow Velocity (ms^{-1})	ω	Rotational Rate ($rads^{-1}$)

References

.

[1] H. Sutherland, D. Berg, T. Ashwill
A Retrospective of VAWT Technology
SAND2012-0304, Sandia National Laboratories (2012), Albuquerque, New Mexico

[2] P. Marsh, D. Ranmuthugala, I. Penesis, G. Thomas
Numerical Investigation of the Influence of Blade Helicity on the Performance Characteristics of Vertical Axis Tidal Turbines
Renewable Energy, 81 (2015), pp. 926-935.

[3] M. Hameed, S. Afaq
Design and analysis of a straight bladed vertical axis wind turbine blade using analytical and numerical techniques
Ocean Engineering, 57 (2013), pp. 248-255

[4] Y. Li, N. Karri, Q. Wang
Three-dimensional numerical analysis on blade response of a vertical-axis tidal current turbine under operational conditions
Journal of Renewable and Sustainable Energy, 6 (2014)

[5] I. Paraschivoiu, N. Dy
A Numerical Study of Darrieus Water Turbine
Proceedings of the Twenty-Second (2012) International Offshore and Polar Engineering Conference, Rhodes, Greece, 2012

[6] J. Tsai, F. Chen
The Conceptual Design of a Tidal Power Plant in Taiwan
Journal of Marine Science and Engineering, 2 (2014), pp. 506-533

[7] G. Rawlings
Parametric Characterization of an Experimental Vertical Axis Hydro Turbine
Master's thesis (2008), University of British Columbia, BC

[8] I. Paraschivoiu
Wind Turbine Design: With Emphasis on Darrieus Concept
Polytechnic International Press (2002), Quebec, Canada

[9] M. Drela
Xfoil Version 6.96
Software, accessed from <http://web.mit.edu/drela/Public/web/xfoil/> [18 December 2014]

[10] C. Masson, C. Leclerc, I. Paraschivoiu
Appropriate Dynamic Stall Models for Performance Predictions of VWATs with NLF Blades
International Journal of Rotating Machinery, 4(2) (1998), pp. 129-139

[11] Ansys Inc.
ANSYS CFX-Solver Theory Guide: Release 13.0
Ansys Inc. (2010), Canonsburg, PA, USA

[12] P. Marsh, D. Ranmuthugala, I. Penesis, G. Thomas
Three-dimensional Numerical Simulations of Straight-Bladed Vertical Axis Tidal Turbines Investigating Power Output, Torque Ripple and Mounting Forces
Renewable Energy, 83 (2015), pp. 67-77

[13] P. Marsh, D. Ranmuthugala, I. Penesis, G. Thomas
Performance predictions of a straight-bladed vertical axis turbine using double-multiple streamtube and computational fluid dynamics
The Journal of Ocean Technology, 8(1) (2013), pp. 87-103

[14] P. Marsh, D. Ranmuthugala, I. Penesis, G. Thomas
Numerical Simulation of Straight-Bladed Vertical Axis Turbines
2nd Asian Wave and Tidal Energy Conference (AWTEC) (2014), Tokyo Japan

[15] P. Marsh, D. Ranmuthugala, I. Penesis, G. Thomas
Three dimensional numerical simulations of a straight-bladed vertical axis tidal turbine

Proceedings of the 18th Australasian Fluid Mechanics Conference (2012), Launceston, Tasmania

[16] F.R. Menter
Two-Equation Eddy-Viscosity Turbulence Models for Engineering Applications
AIAA J, 32(8) (1994), pp. 1598-1605

[17] A.R. Malipeddi, D. Chatterjee
Influence of duct geometry on the performance of Darrieus hydroturbine
Renewable Energy, 43 (2012), pp. 292-300

[18] M.R. Castelli, G. Ardizzon, L. Battisti, E. Benini, G. Pavesi
Modeling strategy and numerical validation for a Darrieus vertical axis micro-wind turbine
ASME 2010 International Mechanical Engineering Congress and Exposition (2010), Vancouver, British Columbia, Canada

[19] Y.M Dai YM, W. Lam
Numerical Study of Straight-Bladed Darrieus-Type Tidal Turbine
Proceedings of the institution of civil engineers, Energy 162(2) (2009), pp. 67-76

[20] S. Lain
Simulation and Evaluation of a Straight-Bladed Darrieus-type Cross Flow Marine Turbine
Journal of Scientific and Industrial Research, 69(12) (2010), pp. 906-912

[21] G.I. Gretton
Hydrodynamic analysis of a vertical axis tidal turbine
PhD thesis (2009), University of Edinburgh, Edinburgh, UK

[22] B.T. Webster
An Experimental Study of an Airfoil Undergoing Cycloidal Motion
MSC dissertation, Texas Tech University, 1978.

[23] J.H. Strickland JH, T. Smith T, K. Sun
A Vortex Model of the Darrieus Turbine: An Analytical and Experimental Study
Final Report (1981), Texas Tech University, Texas.

[24] Unknown
Area and Bending Inertia of Airfoil Sections
MITOPENCOURSEWARE, accessed from <http://ocw.mit.edu/courses/aeronautics-and-astronautics>

[25] Ansys Inc.
ANSYS Mechanical User's Guide: Release 15.0
Ansys Inc. (2013), Canonsburg, PA, USA

[26] P.S Veers
An Approach to the Fatigue Analysis of Vertical Axis Wind Turbine Blades
SAND81-2130, Sandia National Laboratories (1981), Albuquerque, New Mexico